Journal of Thermal Analysis, Vol. 38 (1992) 1701-1728

Special Review

HIGH-PRESSURE DIFFERENTIAL THERMAL ANALYSIS (HP-DTA)
I. Dehydration reactions at elevated pressures in phyllosilicates

*S. Guggenheim and A. F. Koster van Groos**

DEPARTMENT OF GEOLOGICAL SCIENCES, UNIVERSITY OF ILLINOIS AT CHICAGO
CHICAGO, ILLINOIS 60680 U.S.A.

(Received March 17, 1992)

High-pressure differential thermal analysis results are used to describe dehydration reactions for the clay-like materials of Na-rich montmorillonite, K-, Ca-, and Mg-exchanged montmorillonite, kerolite, and a high-pressure phase resembling talc/mica with excess water. Because sealed capsules may be used to contain fluids, it is possible to evaluate the role of H_2O in these reactions. A separate paper (Part II) addresses the use of HP-DTA to understand dehydroxylation reactions in these materials.

Keywords: clay-like materials, dehydration reactions, high-pressure DTA

Introduction

In differential thermal analysis (DTA) at ambient pressure, temperature is the only independent variable. If pressure is added as a variable, a two-dimensional

* Correspondence to: Stephen Guggenheim/A. F. Koster van Groos
Dept. of Geological Sciences, m/c 186
University of Illinois at Chicago
P.O.Box 4348
Chicago, Illinois 60680 USA

John Wiley & Sons, Limited, Chichester
Akadémiai Kiadó, Budapest

pressure-temperature grid becomes available, which may be useful to determine phase relationships, enthalpy of reactions, and other important information. Although high-pressure differential thermal analysis (HP-DTA) techniques are not new (e.g., [1]), early methods were cumbersome. The apparatus described by Koster van Groos [2] has simplified procedures, and experiments now routinely are made to 950°C and 10 kbar. Because the geometry of the sample capsules and their position in the DTA cell are reproducible, DTA thermograms may be compared. In addition, it is possible to investigate solid-fluid assemblages by sealing the sample capsules.

The purpose of this review is to illustrate how HP-DTA may be used to understand the effect of pressure on the role of water in reactions involving clay-like materials. Emphasis is placed on integrating data from DTA experiments and structural data from other methodologies to understand the processes involved in dehydration (Part I) and dehydroxylation (Part II) [3], rather than to review extensively the methodology of high-pressure DTA. A third paper (Koster van Groos, in preparation) is to more fully document HP-DTA techniques and other studies.

Part I briefly reviews the methodology, the structure of the phyllosilicates under study, and the data and the derived structural and thermodynamic relationships for dehydration. Portions of this review are from Koster van Groos and Guggenheim [4].

Experimental method

Apparatus

The main features of the apparatus were described by Koster van Groos [2]. The DTA cell consists of a copper cylinder (Fig. 1) with positions for three capsules. The capsules, fabricated uniformly of Au using extrusion techniques, have a length of 10 mm, a diameter of 3.2 mm, a wall thickness of 0.07–0.08 mm, and a weight of 110–120 mg. A re-entry well of about 1 mm depth accommodates a thermocouple, usually Pt–$Pt_{90}Rh_{10}$, that is spring-loaded to insure thermal contact. The purpose of the re-entry well is to position the thermocouple near the center of mass of the sample. Two capsules contain sample and the third a TiO_2 or Al_2O_3 reference. The copper cell-thermocouple assembly is placed in an internally heated pressure vessel similar to the one described by Holloway [5].

The temperature of the sample capsules is obtained from the temperature of the reference and corrected using the differential temperature. The correction can be as high as 3°C, but it is usually less than 1°C. Because of this correction, the nature of the reference is not important as long as it is inert in the temperature range of interest. The DTA signals are recorded on a strip-chart recorder which has a maximum resolution of 100 nV or ~0.02°C. Pressures to 5 kbar are measured to within 0.5% with low-, medium-, and high-pressure Bourdon-type

calibrated Heise gauges. Above 5 kbar, a Harwood manganin cell is used, which is calibrated against the Heise gauges. Most experiments are run at a heating rate of 20 deg/min, using a programmable controller. The system is regularly calibrated at different pressures against the low quartz–high quartz inversion [6, 7]. The corrected temperatures are believed accurate to within 1°C.

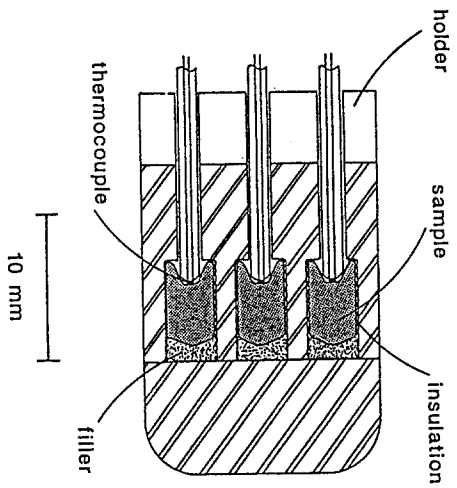

Fig. 1 Copper DTA cell with positions for two samples and a reference

An important feature of the method is that the geometry of the capsules and their position in the cell are reproducible, allowing comparison of the DTA signals. Furthermore, the capsules may be open or welded shut and studies in closed systems are possible. Using this sample geometry, the onset and termination of the peak representing the low-high transition of 4 mg quartz, well-mixed with a 20 mg sample, extend over a 3°C temperature interval, with a sharply defined peak in approximately the middle of this interval. No visible effects of smearing out of the signal have been detected. Thus, thermal gradients within the sample are likely to be small, probably less than 1° at 573°C. The reproducibility of the temperatures is within 0.5°C.

Sample preparation and characterization

The starting materials used in the DTA studies described below are a Na montmorillonite from the Newcastle Formation of Crook County, Wyoming (Clay Mineral Society Source Clay SWy-1, see [8]), kerolite from the Carter's mine, Madison County, North Carolina [9] and a synthetic talc- and mica-like phase with excess water relative to talc [10, 11].

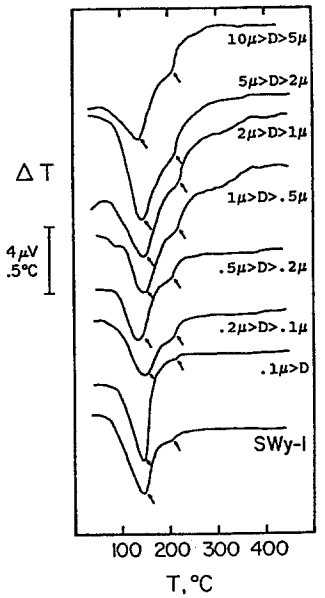

Fig. 2 DTA curves at 1 atmosphere of SWy-1. Shown are patterns of bulk SWy-1 and seven hydraulic diameter fractions (D). Arrows point at two separate dehydration reactions

All starting materials were sieved to pass 200 mesh. The expandable clays were stored over a saturated aqueous solution of $Mg(NO_3)_2 \cdot H_2O$ (55% relative humidity); all other samples were stored in a desiccator. Grain size effects of the montmorillonite on the DTA curves were investigated at 1 atmosphere by analyzing a sequence of eight different hydraulic fractions, ranging from >10 μm to <0.1 μm, Fig. 2 [12]. It does not appear to affect the results significantly, although the peak of the finest fraction is somewhat sharper than in the other fractions. Therefore, only the finest fraction was used in the series of experiments discussed here. It should be noted, however, that scanning electron microscopy (SEM) showed that the coarse fractions of SWy-1 are composed of aggregates of smaller crystals and that the crystal size itself does not vary significantly between the different fractions (Koster van Groos, unpublished). In order to determine the effect of the interlayer cation on water-loss (or hydroxyl-loss as given in Part II) reactions, SWy-1 was cation-exchanged with K, Ca, or Mg, using 1*N* chloride solutions at ambient conditions, followed by six washings with distilled water and drying in air. These exchanged montmorillonites will be referred to as KSWy-1, CaSWy-1, and MgSWy-1. Because SWy-1 is already Na-rich, it was not further cation exchanged with Na.

X-ray and chemical analysis of the samples were made to determine the mineralogical and chemical composition. Their chemistry is given in Table 1.

Table 1 Chemical analyses of starting materials[1]

	SWy-1[2]	SWy-1[3]	KSWy-1[3]	CaSWy-1[3]	MgSWy-1[3]	Ker[4]
SiO_2	62.9	66.4	64.3	62.4	65.3	62.98
TiO_2	0.13	0.12	n.a.	n.a.	n.a.	n.a.
Al_2O_3	19.4	23.7	23.16	24.1	23.5	.07
Fe_2O_3	3.6	n.a.	n.a.	n.a.	n.a.	.51[5]
FeO	.22	4.19[5]	4.75[5]	4.16[5]	4.23[5]	n.a.
MgO	2.92	2.77	3.46	3.39	5.79	30.19
CaO	1.76	1.05	.40	4.33	.27	.17
Na_2O	1.53	.58	.0	.0	.0	.01
K_2O	.54	.16	3.75	.04	.16	.14

n.a. not analyzed

[1] Totals are not given because of varying H_2O content

[2] Bulk sample analyses averaged from two analyses each as given by [8]

[3] Electron microprobe analyses of glass obtained from <0.1μm hydraulic fraction of SWy-1 and exchanged SWy-1

[4] Kerolite from Carter's Mine [9]

[5] As total iron

Differential thermal analysis

The generation of a thermal signal depends strongly on the kinetics of the reaction. Thus, DTA is limited to reactions that are reasonably fast. Furthermore, DTA and other thermal analytical data cannot distinguish between stable or metastable equilibria. Reversibility of a reaction is insufficient evidence to determine the nature of the equilibrium. For example, a metastable reaction may be readily reversible, e.g., the dehydroxylation of muscovite [13], whereas a stable melting reaction in silicate systems may not be reversed easily.

In the interpretation of a DTA pattern, the temperature of the extrapolated onset of a peak, the peak temperature, the extrapolated peak temperature using the tangent of the main slope of the peak, the temperature of the intersection of the extrapolated limbs of a peak, or other segments of the peak have been used to determine the reaction temperature, the enthalpy of reaction, and information on the kinetics of the reaction. There is a consensus, that the reaction rate is the highest at the peak temperature. To assess these aspects of a DTA peak, possible changes in the conditions during the reaction and their effects must be considered. For example, in the low quartz-high quartz inversion, the activity of the phases is not or only slightly affected during the reaction. During a dehydration, dehydroxylation, or decarbonation reaction, however, the fugacity of the evolving gas phase may increase during the reaction. In general, this causes the reaction temperature to increase, resulting in a broader peak.

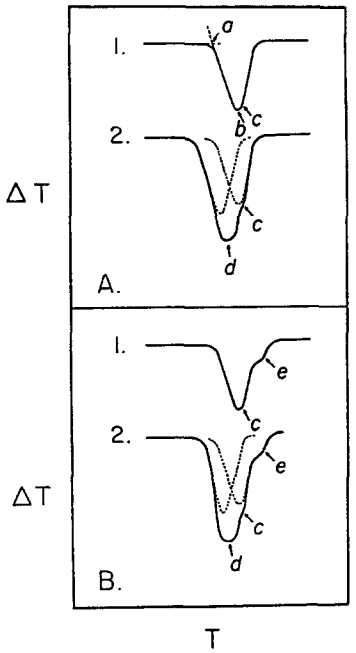

Fig. 3 *A*: Curve (1) shows an idealized DTA pattern of a smectite. Point (*a*) represents the onset of the reaction, point (*b*) the peak temperature, and point (*c*) the temperature at which the reaction is almost completed and the curve starts its rapid return to the baseline. Curve (2) shows the effect of the presence of water. Point (*d*) represents the combined peak. Point (*c*) is a shoulder in the curve, and is at the same temperature as point (*c*) in curve (1). *B*: Idealized patterns as in (*A*), but the smectite has two dehydration reactions

Another complication arises if more than one reaction occurs at approximately the same temperature. This is illustrated in Fig. 3. Curve (1) in Fig. 3*A* shows a simplified dehydration peak of a smectite. The extrapolated onset (*a*), the peak (*b*), and the point at which the reaction is virtually completed (*c*) define the signal. Curve (2) shows the result when a second reaction occurs simultaneously, such as the boiling reaction of water, hereafter referred to as $(L, V)_{H_2O}$. The combined peak has an apex at (*d*), which does not represent either $(L, V)_{H_2O}$ nor the dehydration peak of the smectite; e.g., compare the dashed lines which show the individual peaks. In order to determine the onset of the smectite dehydration peak on curve (2), the additional peak must be subtracted. Although with known or ideal peak shapes deconvolution methods can be used, in most systems the size and shape of additional peaks are difficult to assess and the determination of the onset of the second reaction becomes impossible. Location of the apex of an individual peak is often simple, because the corresponding rapid change in reaction rate results in a well-defined inflection point on the limb of the combined peak. In

some cases the reaction is more complex. For example, in montmorillonite, often two dehydration peaks are observed (Fig 2, 4) and this may be illustrated ideally in Fig. 3*B*, curve (1). With water present, the combined peak is encountered at (*d*) in curve (2), and the two dehydration reactions are evident as shoulder peaks at (*c*) and (*e*). Examples of this (Fig. 4) show two dehydration peaks of SWy-1 added to the peak of the reaction $(L, V)_{H_2O}$ [12]. Because in these examples the $(L, V)_{H_2O}$ peak dominates, the temperatures of the apex of the combined peak coincide with the *PT* conditions of the boiling reaction. The peak temperatures of the two dehydration reactions are shown by a break or a change in the slope toward the baseline, similar to what is given in Fig. 3*B*. A series of experiments at pressures to 50 bars did confirm that the temperature of these changes in slope is reproducible and is the same as the peak temperature in runs with only smectite present.

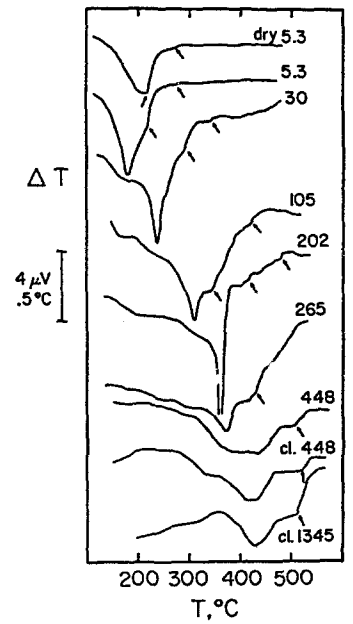

Fig. 4 HP-DTA patterns of SWy-1 in runs using open and closed (*c*1) capsules. The arrows indicate the temperature at which the dehydration reaction is almost completed, compare point (*c*) in Fig. 3*B*. The large low-temperature peak represents the boiling reaction of water (*L*, *V*). Broadening of this peak above the critical point indicates a second order transition from a liquid-like to a vapor-like phase [12]. Run pressures are in bars

Additional experimental considerations

Significant differences in dehydration temperatures of a particular smectite have been reported. These differences are attributed to a varying H_2O fugacity (f_{H_2O})

in the sample, caused by small differences in the experimental procedure [12]. For example, heating larger or more compacted smectite samples may result in an increase of f_{H_2O} within the sample during a dehydration reaction, which would raise the dehydration temperatures by up to several tens of degrees centigrade. This effect is illustrated in Fig. 5. A DSC analysis of the interlayer water-loss in MgSWy-1 was made using two identical samples. The only difference between the two experiments is that one sample-holder lid was left ajar. In the closed pan, evolving H_2O vapor resulted in a slightly higher P_{H_2O} around the sample, and peak temperatures increased about 15°C, establishing that even small differences in P_{H_2O} can produce significant variations in observed temperatures.

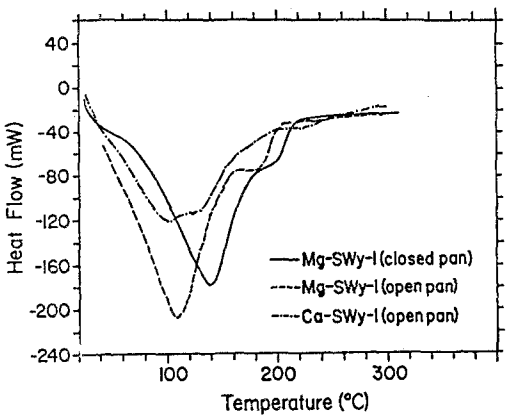

Fig. 5 DSC diagrams for CaSWy-1 and MgSWy-1. The shift of the pattern of MgSWy-1, using an open pan relative to a closed pan, is attributed to the partial pressure of H_2O. Note the two peaks for CaSWy-1 between 100° and 140°C analyst: P. van Krieken, University of Utrecht (from [16])

In our HP-DTA system, thermal analysis is carried out in open or closed systems at pressures to 10 kbars. In the study of an open system, i.e. open capsules, P_{H_2O} may not equal P_{total} when investigating dehydration (or dehydroxylation) reactions. At low pressure and elevated temperatures, sealed capsules cannot be used; they fail because the molar volume of H_2O vapor is too high. However, the volume of H_2O vapor generated during the early stages of dehydration of smectite in open capsules appears sufficient to flush the Ar gas pressure medium out of the capsule. In these experiments, it is assumed that the gas phase enveloping the sample approached pure H_2O. In order to limit mixing of the evolving water vapor with the Ar gas, which would reduce the f_{H_2O} near the sample, the space in the capsule above the sample was tightly filled with an inert fiber, such as quartz glass wool. In these experiments, conditions of $P_{H_2O} = P_{total}$ can be maintained at temperatures to ~300°C at pressures to about 50 bars.

In runs between 50 and 200 bars, the addition of 5–30 wt% water at the bottom of the capsule before introducing the sample was necessary to maintain $P_{H_2O} = P_{total}$. Where not enough water was added or where water was lost prior to or during a run, lower and non-reproducible dehydration temperatures were found. In runs with sufficient water present, the endothermic peak of $(L, V)_{H_2O}$ interfered with the smectite peaks, as was discussed above. However, the P–T conditions of $(L, V)_{H_2O}$ are well-known [14] and the related peak is identified readily.

Closed capsules can be used successfully if the pressure within the capsule does not exceed the external pressure. In these experiments, typically 5–10 wt% water was added to the starting material to insure that $P_{H_2O} = P_{total}$. Above the critical pressure of water, the liquid-vapor transition occurs over a temperature interval. Thus, the resulting peak is observed over an increasingly wide temperature range with a further increase in pressure.

In the dry runs, the density of the sample was controlled by slightly compressing the sample with a constant force. In open-capsule runs with water present, water was pipetted into the capsule before introducing the sample, to ensure that during the run the H_2O gas from the evaporating water encloses the sample. In most runs, about 20–30 mg of sample was used. The amount of both water and sample were determined by weight. Sealed capsules were checked for leaks before and after each experiment. If a capsule lost weight during a run, it was assumed that $P_{H_2O} < P_{total}$; their results were either not used or used only qualitatively. Run products were examined microscopically and by X-ray diffraction methods.

Structural aspects of phyllosilicates

Before the results of HP-DTA are discussed, relevant aspects of the materials investigated need to be considered. The structures of layer silicate minerals (Fig. 6) are dominated by planes of octahedrally-coordinated and tetrahedrally-coordinated cations. The octahedral cation and nearest-neighboring anions comprise the octahedral sheet as the result of two-dimensional linkage through the sharing of polyhedral edges. A hexagonal-based tetrahedral sheet is formed by the linkage of TO_4 groups (T = Si, Al) in which individual tetrahedra share three corners (basal oxygens) with tetrahedral neighbors. The hexagonal character of the sheet results from the two-dimensional linkage of tetrahedra, which form sheets of six-fold rings. The fourth tetrahedral corner (apical oxygen) is not involved in sharing corners with other tetrahedra, but is involved in the joining of the tetrahedral and octahedral sheets. The apical oxygen forms a portion of a common plane of junction between the tetrahedral and octahedral sheets, and belongs to both the octahedral cation coordination and the tetrahedral cation coordination. Different assemblages may form depending on the number of component sheets

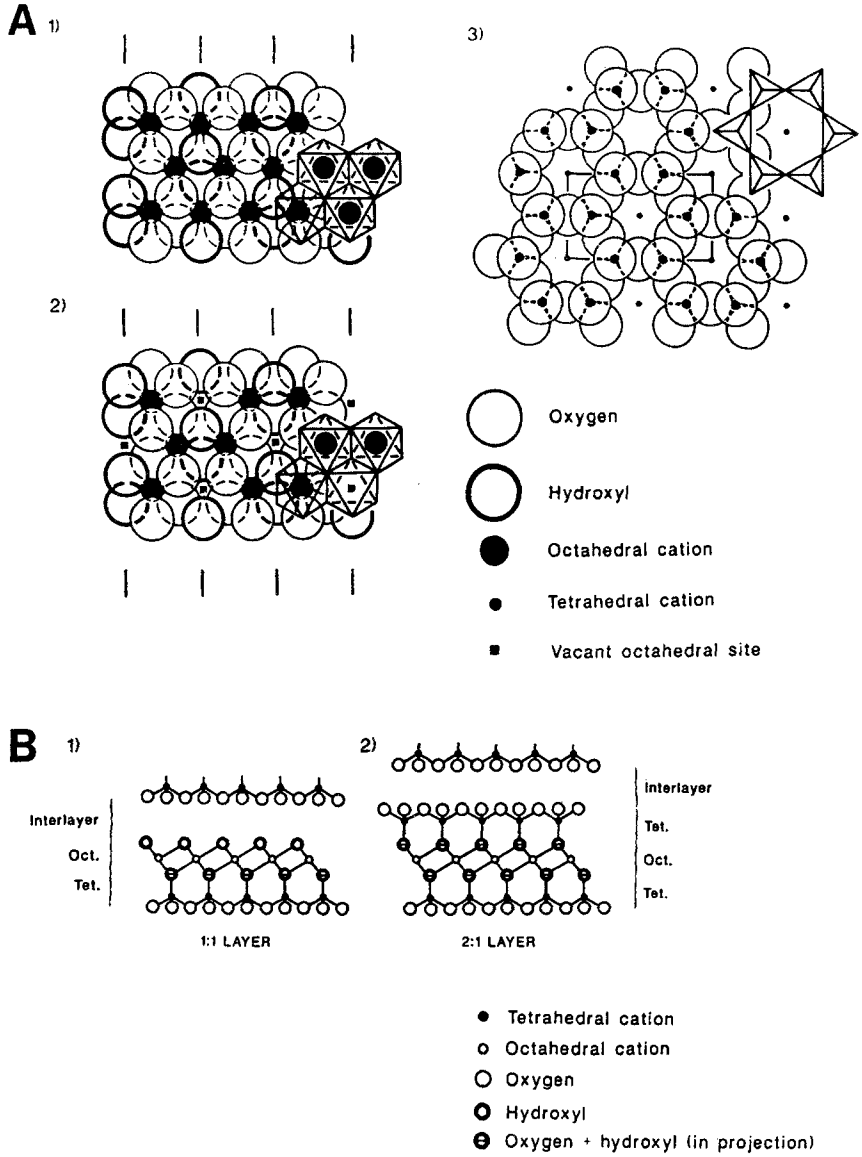

Fig. 6 *A*: A trioctahedral sheet (1), a dioctahedral sheet (2), and a tetrahedral sheet (3) are shown in plan. *B*: These sheets may be linked laterally to form either 1:1 layers (1) or 2:1 layers (2)

that link together. If one tetrahedral sheet is linked to an octahedral sheet, a 1:1 layer results, whereas if two tetrahedral sheets oppose each other with the octahedral sheet between, a 2:1 layer forms (Fig. 6*B*).

Although two apical oxygens per attached tetrahedral sheet form the coordination about each octahedral cation additional anions, typically OH or less commonly F, are needed to complete six-fold coordination. For example, for 2:1 layer silicates, two additional OH groups are required. The OH groups are located on opposing sides of the octahedral cation with each at nearly the same level along the *c* axis as the apical oxygens and in the center of the six-fold silicate ring. Consequently, the two OH groups are energetically very similar. However, 1:1 layer silicates have only one attached tetrahedral sheet and such a sheet can supply only one OH group per octahedral cation in an analogous manner. It is necessary, therefore, to have an additional plane of OH groups that complete the 1:1 layer. Thus, in 1:1 layer silicates, there are two very different types of OH groups; OH groups located within six-fold rings and others which reside on an internal surface parallel to the (001). The latter form long (~2.9Å) hydrogen bonds across the interlayer to the basal oxygen of the next 1:1 layer. The location of the OH group in the layer silicate structure and, therefore, its bonding energy determine its response to temperature and pressure changes.

If the 1:1 or 2:1 layers are not electrostatically neutral, adjacent layers may be separated by additional cations, hydrated cations, metal-hydroxyl octahedral sheets, organic compounds, or various other interlayer material to offset the residual charge on the layer. In addition to the type of layer, phyllosilicates are often classified on the basis of this interlayer material. For example, 2:1 layer-type phyllosilicates with interlayer material consisting of complete metal-hydroxyl octahedral sheets, have a chlorite structure. In contrast, if hydrated cations comprise the interlayer, a smectite (including montmorillonite) structure results. Structures intermediate between chlorites and smectites, those with hydrated cations with two H_2O planes that may be thought of as an incomplete octahedral sheet configuration, are known as vermiculites (Table 2).

Interlayer material is important in understanding thermal stability for two reasons: (*a*) if water molecules or OH groups are located in the interlayer region, the stability of these molecules or groups will be different than if they occur within the 1:1 or 2:1 layer; and (*b*) interlayer material may interact with the OH groups located within a 2:1 layer, as is the case with the interlayer cation in a mica, which resides partially within the silicate ring and is close enough to the OH groups to influence thermal behavior. In special cases, interlayer material may migrate from the interlayer region into the 2:1 layer, thereby affecting the thermal stability of the OH groups within a 2:1 layer (e.g., Fig. 6).

Often, H_2O is sorbed onto the surface of fine particles as there is a finite charge associated with broken bonds on crystal surfaces. Such surface effects are considerable for clay minerals because, in addition to the surfaces bounding the individual particle, some clay minerals have 'internal' surfaces (an atomic plane

at the interlayer) that are readily accessible to H_2O molecules residing in the interlayer. Usually, H_2O-loss from either surface can be distinguished on the basis of the response to thermal effects, with H_2O-loss from external planes occurring at lower temperatures (less than about 100°C) than from internal surfaces.

Table 2 Classification of 1:1 and 2:1 layer silicates, after [30]

Layer type	Group (x = charge per $O_{10}(OH)_2$ formula unit)	Sub-group
1:1	Serpentine-kaolin	Serpentines
	($x \sim 0$)	Kaolins
2:1	Talc-pyrophyllite	Talcs
	($x \sim 0$)	Pyrophyllites
	Smectite	Saponites
	($x \sim 0.2$–0.6)	Montmorillonites
	Vermiculite	Trioctahedral vermiculites
	($x \sim 0.6$–0.9)	Dioctahedral vermiculites
	Mica	Trioctahedral micas
	($x \sim 1.0$)	Dioctahedral micas
	Brittel mica	Trioctahedral brittle micas
	($x \sim 2.0$)	Dioctahedral brittle micas
	Chlorite	Dioctahedral chlorites
	(x variable)	Di, trioctahedral chlorites

Therefore, H_2O occurs in layer silicate minerals either as OH groups (referred to as strongly-bonded water) or as H_2O molecules. The former may be present at the junction between the tetrahedral and octahedral sheets in either 1:1 or 2:1 layers, they may be associated with the octahedra to complete six-fold coordination at an 'internal' surface, or they may be associated with either a partial or complete octahedral interlayer. In contrast, H_2O molecules are located in the interlayer (hydrated cations) or on exterior surfaces. They tend to be poorly-bonded to the structure. Thermal analytical techniques offer a methodology to distinguish between the various H_2O or OH constituents on the basis of differences in site energy as determined by their response to thermal effects. H_2O-loss involving

poorly-bonded interlayer water is discussed below as a 'dehydration' reaction whereas loss of structural water (OH) is termed 'dehydroxylation' reaction (Part II). H_2O-loss from external planes are considered also under dehydration. An unusual synthetic phase, known as the '10Å phase', has excess water in the interlayer in the form of either H_3O^+, H_2O, or O^{2-} with two resonating protons; it is discussed below in the section on dehydration reactions.

Dehydration reactions

Montmorillonite

Montmorillonite is approximately $(M_ynH_2O)(Al_{2-y}Mg_y)Si_4O_{10}(OH)_2$ where *M* is Na, K, Mg, Ca, and other exchangeable cations. In montmorillonite, because the interlayer cation can be exchanged without affecting the chemistry of the 2:1 layer, the relation between various cations and the *P–T* conditions of interlayer

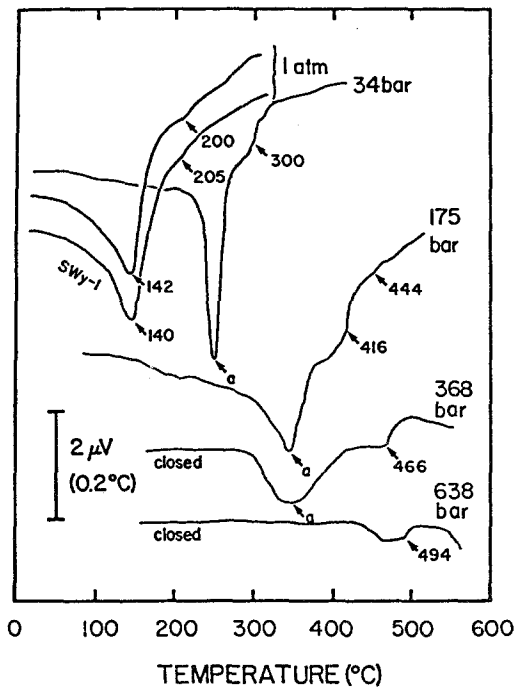

Fig. 7 HP-DTA patterns for the dehydration reaction of KSWy-1, using open and closed capsules. For comparison a run with SWy-1 at 1 atm is included. The arrows indicate the temperature at which each dehydration reaction is virtually complete, compare points (*c*) in Fig. 3*B*. The peak labelled 'a' represents the boiling reaction of water [15], (*L*, *V*)

water-loss can be investigated. From the results, the enthalpy of dehydration, using the van't Hoff equation, may be obtained. The advantage of this method over calorimetry is that neither purity nor quantity of the sample affects the data. Therefore, the *P-T* relations of the dehydration reactions of Na montmorillonite (SWy-1), KSWy-1, CaSWy-1, and MgSWy-1 can be determined [12, 15, 16].

HP-DTA data

Figures 4, 7 and 8 give representative HP-DTA patterns for SWy-1 and the Ca-, Mg-, K-exchanged samples. In experiments at elevated pressures, the capsules contained added water to maintain $P_{total} = P_{H_2O}$. In these runs, the peak representing $(L, V)_{H_2O}$ dominates; the dehydration peaks of the montmorillonite are present on the high-temperature shoulder. With open capsules, the H_2O peak is usually asymmetric (e.g., the wet 5.3 bar run, Fig. 4) because of evaporation during heating. When $(L, V)_{H_2O}$ is reached, boiling of the remaining liquid generates a sharp peak (e.g., 34 bar run, Fig. 7). The shapes of the $(L, V)_{H_2O}$ peaks for the closed-capsule runs are similar, although when the critical pressure of water is exceeded the peak becomes broad and less well-defined (e.g., 368 and 638 bars, Fig. 7).

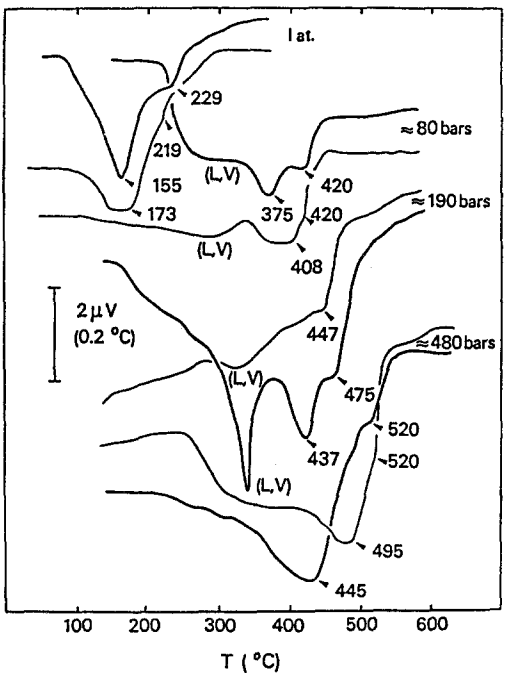

Fig. 8 HP-DTA patterns for the dehydration reaction of CaSWy-1 (light lines) and MgSWy-1 (heavy lines), using open and closed capsules. The arrows indicate the temperature at which each dehydration reaction is almost completed, compare points (*c*) in Fig. 3*B*. The peak labelled (*L, V*) represents the boiling reaction of water [16]

In these patterns the dehydration temperatures can be determined with little ambiguity. In most cases two peaks are present (e.g., Fig. 8, at 190 bars) in addition to the $(L, V)_{H_2O}$ peak, although occasionally only one peak was identified (e.g., at 80 bars). Note that there are significant differences in patterns from different interlayer compositions. For example, in runs with KSWy-1 the peak for the second dehydration is much smaller than for the other samples. Koster van Groos and Guggenheim [12] suggested that the break in slope on the high temperature side of the $(L, V)_{H_2O}$ peak, or a small shoulder peak, may be used as an indication that the dehydration reaction is essentially complete. Where the second dehydration peak is small, as in KSWy-1, it is important to verify that the break in slope is consistent in different runs. Thus, all runs in which it can be assumed $P_{H_2O} = P_{total}$, i.e., dry runs at low pressures, wet runs at intermediate pressures, and wet runs in sealed capsules at high pressures, must yield reproducible and consistent data.

Discussion

In these montmorillonites the higher temperature peak is noticeably smaller than the low temperature peak. Previous DTA and infrared (IR) evidence (e.g., [17, 18, 19]) suggests that interlayer water is not bonded equally and that a distinction can be made between strongly bonded water molecules *vs* weakly bonded water molecules. Following this view, the two HP-DTA peaks may be related to the expulsion of the weakly bonded water (low-temperature peak) and, after the loss of outer hydration shells from the interlayer cations, to a second H_2O-loss event. The latter, then, involves the inner hydration shell of the interlayer cation and is dependent not only on bonding effects of the interlayer cation but also on interactions with the 2:1 layer. Because in these experiments the chemistry of the 2:1 layer was the same, the difference must relate to the nature of the interlayer cation.

P–T relations of the dehydration reactions of the Ca and Mg exchanged montmorillonites are shown in Fig. 9. These reactions, as well as the reactions involving the Na-rich and K exchanged montmorillonites (not shown), follow the general shape of the boiling curve for water, $(L, V)_{H_2O}$. Dehydration in several runs occurred at temperatures that are anomalously low. We interpreted this as evidence that in these runs $P_{H_2O} < P_{total}$. The large effect of small differences in f_{H_2O} on the dehydration temperature previously observed (e.g. Fig. 5) is explained by the near-horizontal slope of the dehydration curves at low pressures. The temperatures and curvature of the first dehydration (low temperature) reaction varies for the different interlayer cation, whereas the temperatures of the second dehydration (high temperature) reaction appear less affected.

Determination of the enthalpy of a reaction at a single pressure on the basis of the area of a peak is possible if all variables involving a reaction can be evaluated accurately [20]. This is difficult, because the calibration of the instrument may vary with temperature, reaction rate, and the size and thermal conductivity of the

sample. Calorimetric methods using the determination of the heat of formation of the reactants and products are generally much more precise. However, in fine-grained naturally-occurring material, such as clay, the accuracy of calorimetric methods may suffer from impurities (e.g., colloidal quartz).

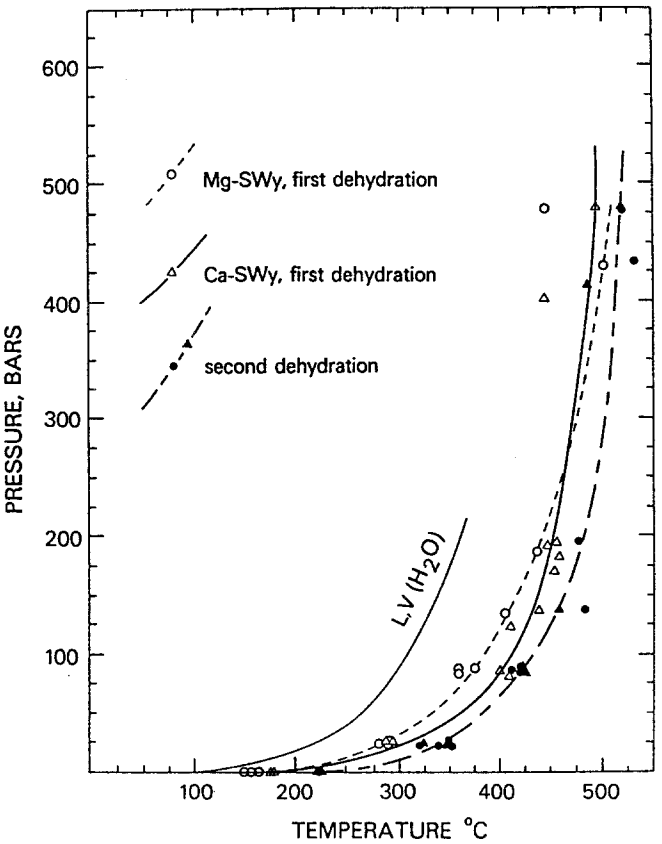

Fig. 9 P–T projections of the dehydration reactions of CaSWy-1 and MgSWy-1. $(L, V)_{H_2O}$ is the boiling curve of water [14]

A fundamentally different approach is to determine the enthalpy of reaction from the *P–T* relation of a reaction, using a modified version of the van't Hoff equation, $\ln P_2 - \ln P_1 = (\Delta H / R)(1/T_2 - 1/T_1)$. The modification reflects the dominance of the volume change caused by an evolving gas in the reaction (e.g., [21]). Consequently, the volume change of the solid phases on ΔV is ignored. Furthermore, the equation can only be used if the fugacity coefficient, Γ_{H_2O} is constant (here assumed to be 1) and the difference in heat capacities ΔC_p is approximately zero. Its use is illustrated by a plot of $(L, V)_{H_2O}$ using data from the

Steam Tables [14], which shows that, although Γ_{H_2O} varies considerably over the P–T range, the plotted data lie on a straight line (Fig. 10). Its slope yields the enthalpy of evaporation $\Delta H_{ev} = 39.5$ kJ/mole at 1 bar and 100°C. If a 2% adjustment is made (because $\Gamma_{H_2O} = 1$ was assumed rather than 0.98 [22]), $\Delta H_{ev} = 40.29$ kJ/mole, which is very close the value of 40.886 kJ/mole, determined by calorimetry [23].

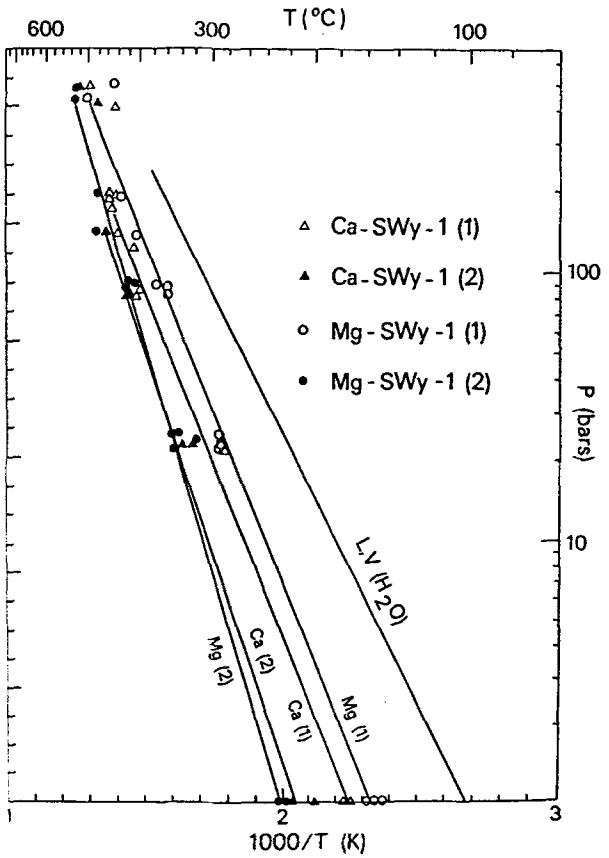

Fig. 10 A ln$P$–1000/T projection of the dehydration reactions of CaSWy-1 and MgSWy-1. (1) and (2) refer to the first and second dehydration reaction, respectively. The boiling curve of water, $(L, V)_{H_2O}$ [14] is shown for comparison

For each montmorillonite the enthalpy of dehydration at 1 bar, ΔH_{dh}, was obtained from the slope of the dehydration reactions in ln$P$–1/T space (Fig. 10). A greater weight was given to the 1 bar data and to the results yielding the higher dehydration temperatures, because these are more likely to represent run conditions at $P_{H_2O} = P_{total}$.

Table 3 Enthalpy (kJ/mol) of dehydration and interlayer water-loss in layer silicates

Phase	Reaction	ΔH_{dh}	ΔH_{iw}
SWy-1	first dehydration	46.8±0.5	7.8±0.5
	second dehydration	62.9±2	27.1±2
KSWy-1	first dehydration	46.2±0.5	7.8±0.5
	second dehydration	56.7±2	19.8±2
CaSWy-1	first dehydraton	49.5±0.5	12.1±0.5
	second dehydration	58.2±2	22.6±2
MgSWy-1	first dehydration	49.3±0.5	11.1±0.5
	second dehydration	66.2±2	31.1±2
Kerolite	sorbed	41.2±1	1.0±1
	dehydration	45.6±2	5.8±2
10Å phase	dehydration	225.0±20	200.0±20

The enthalpy of a reaction is the total heat involved in the breaking and forming of bonds. Thus, $\Delta H_{dh} = \Delta H_{iw} + \Delta H_{ev}$, where ΔH_{iw} is the molar enthalpy of the removal of interlayer water and represents the bonding of H_2O to the structure. ΔH_{iw} can be obtained after ΔH_{ev} is evaluated by extrapolating the ≤1 bar data for $(L, V)_{H_2O}$ [14] to the temperature of dehydration at 1 bar. Values for ΔH_{dh} and ΔH_{iw} of these montmorillonites are given in Table 3. ΔH_{iw} for the first (low temperature) dehydration event is the same in SWy-1 and KSWy-1. Similarly, differences in ΔH_{iw} for the divalent interlayer cations are small. This appears reasonable because interlayer cations cannot greatly influence the voluminous and weakly bonded second and third nearest neighbor molecules (i.e., the outer hydration shell). ΔH_{iw} for the second dehydration reaction is much higher and more dependent on the nature of the interlayer cation, e.g. compare ΔH_{iw} for the second dehydration of KSWy-1 and MgSWy-1. It involves more tightly bound H_2O (inner hydration shell), which is affected by the interlayer cation and the effects of charge undersaturated basal oxygens on the surface of the 2:1 layer (for any tetrahedron with Al substitutions for Si). As was mentioned before, the 2:1 layer was constant in all experiments and, therefore, the differences in ΔH_{iw}, for the second reaction must be attributed to the effect of the interlayer cation only. Thus, the bonding of the inner hydration shell of H_2O molecules is related to both size and charge of the interlayer cation.

Table 4 Estimated number of water molecules/interlayer cation in SWy-1, KSWy-1, CaSWy-1, and MgSWy-1

Cation	Total water	Total water	Estimated distribution	
	wt%	molecules	1st reaction	2nd reaction
Na	9	4–5	4–4½	1/2
K	6	3–4	3–4	<< 1/2
Ca	16	13	12	1
Mg	16	13–14	11	2

The ratio of H_2O molecules/interlayer cation in these montmorillonites were estimated from TG data, see Table 4 [16]. The SWy-1 starting material was not Na exchanged, although it was purified and size-fractionated. Therefore, its H_2O content may not be representative of a Na-exchanged SWy-1.

Physical model

The disparity in the enthalpy for the second dehydration reaction (c.f., KSWy-1: ΔH_{iw} = 19.8 kJ/mol; MgSWy-1: ΔH_{iw} = 31.1 kJ/mol) suggest important differences in the bonding of the H_2O molecules of the inner hydration shell. It probably involves both the effects of the interlayer cation and the basal plane surface. For example, the high value of ΔH_{iw} of the second dehydration for MgSWy-1 indicates that these water molecules are bound to the interlayer more tightly than H_2O molecules associated with the other interlayer cations. This interpretation is consistent with the relatively high temperature of the reaction (~225°C for MgSWy-1 *vs.* ~215°C (SWy-1), ~210°C (CaSWy-1), ~195°C (KSWy-1)). One explanation is that Mg simply holds the H_2O molecules more tightly in the interlayer. Alternatively, the results may suggest that a portion of the Mg^{2+}-H_2O complex is capable of partially entering the silicate rings of the 2:1 layer, thus bonding a H_2O molecule more tightly to the structure. Because water is polar, this arrangement would serve also to help charge-compensate the undersaturated basal oxygens associated with Al-substituted tetrahedra. Conversely, large interlayer cations, such as K, would be more effective in preventing H_2O molecules from partially entering the silicate rings.

Kerolite

Kerolite, approximately $Mg_3Si_4O_{10}(OH)_2 \cdot nH_2O$ where n= 0.8–1.2, is a rare phyllosilicate. In contrast to montmorillonite, it does not have either swelling or cation-exchange capabilities. Brindley *et al.* [9] showed from IR data and rehydration experiments that H_2O in kerolite resides on layer surfaces and edges (adsorbed molecular water). Also, a small amount of H_2O may be located within the interlayer region, perhaps within the hexagonal rings of the tetrahedral sheet.

Although kerolite differs from montmorillonite by its trioctahedral chemistry, it is similar to montmorillonite by having adsorbed water. Thus, the non-swelling behavior of kerolite allows the study of surface properties of phyllosilicates without the interference of layer swelling.

HP-DTA data

Dehydration temperatures in kerolite almost coincide with the boiling of water. Therefore, no water could be added to the sample in the experiments. Figure 11 shows two open-capsule runs at low pressures and three closed-capsule runs at higher pressures [24]. The broad peaks are either indicative of an increase of P_{H_2O} during dehydration, of variations in the location of the dehydrating H_2O causing a series of separate thermal events, or of a combination of these. Because the amount of evolving H_2O (8 wt%) is high, it appears unlikely that P_{H_2O}

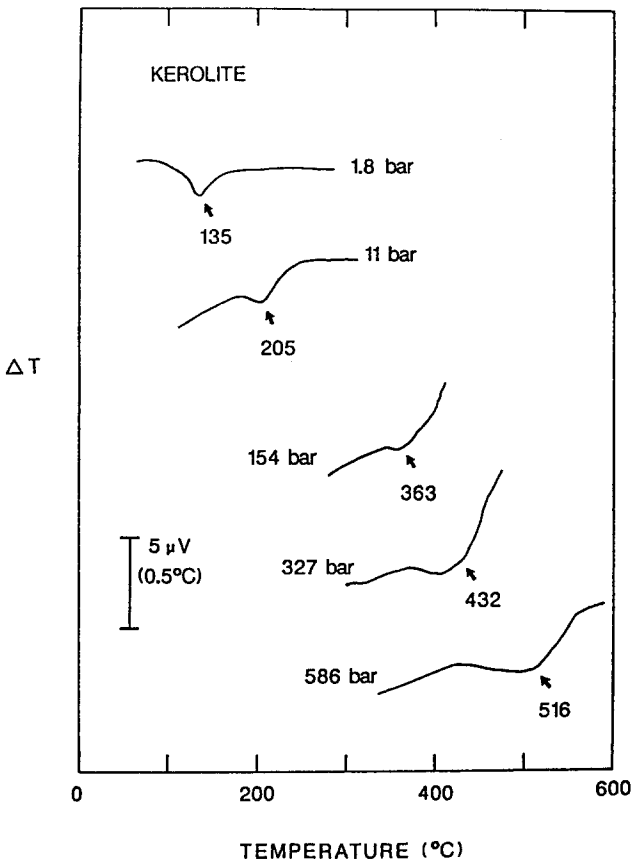

Fig. 11 HP-DTA patterns of the kerolite dehydration reaction. Runs at 1.8 and 11 bars are from open-capsule runs. The others are from closed-capsule runs. The arrows indicate the peaks

changed significantly during dehydration. Furthermore, previous workers have recognized several locations for H_2O. If it is assumed that the released H_2O vapor in low-pressure runs displace Ar from the open capsules, then $P_{H_2O} = P_{total}$ in these runs.

Discussion

The variation of PT relations of the dehydration is monotonic [24], see Fig. 12. Note that the high-pressure open-capsule runs resulted in anomalously low temperatures. The close proximity of the dehydration curve of kerolite to $(L, V)_{H_2O}$ suggests that the presumably adsorbed H_2O is weakly bonded. The peak temperatures, representing the loss of the bulk of this H_2O, generate a straight line (Fig. 13) in $\ln P - 1/T$ space, yielding a $\Delta H_{iw} = 1.0 \pm 1$ kJ/mole. Obviously, this water is weakly bonded to the layer surfaces of kerolite. Considering that the broad peak may represent several thermal events, the final dehydration may occur where the temperature of the DTA signal returns to base line (extrapolated return

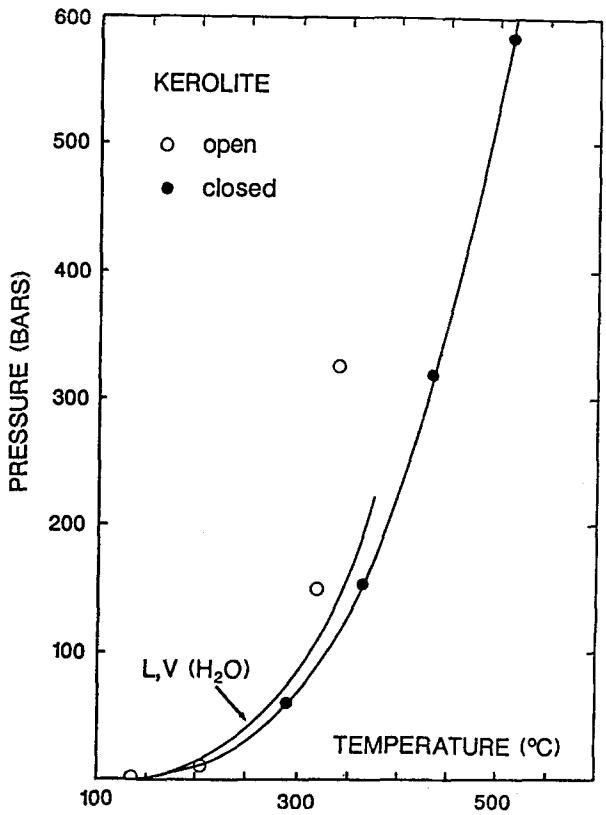

Fig. 12 P–T relations of the kerolite dehydration reaction. The boiling curve of water [14] is shown for comparison

temperature). The associated enthalpy for the final dehydration, ΔH_{iw}, is equal to 5.8± 2 kJ/mole. This value appears reasonable for interlayer water in silicate rings of a neutral 2:1 layer in the absence of an interlayer cation; e.g. compare the enthalpy values of 7.8 to 12.1 kJ/mole for second nearest-neighbor water molecules in the interlayer of montmorillonites (Table 3).

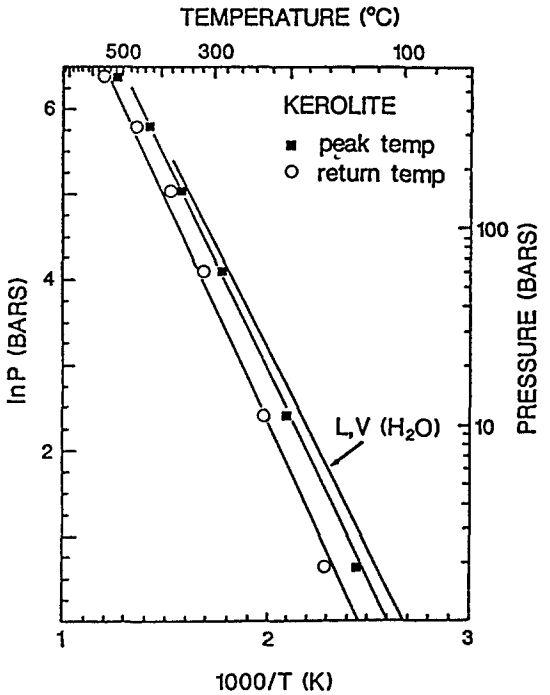

Fig. 13 A ln$P$–1000/T projection of the sorbed water-loss and the dehydration reaction of kerolite. The boiling reaction $(L, V)_{H_2O}$ [14] is shown for comparison

10Å phase

An unusual, synthetic, high-pressure phase, referred to as the '10Å phase', was synthesized by Sclar *et al.* [25]. The phase was recently studied by HP-DTA [11]. The phase is chemically similar to talc but contains excess water in the interlayer. It is believed to be stable at pressures between 32 and 95 kbar and temperatures between 375°C and 535°C, Bauer and Sclar [26, 27] suggested compositions of either $(H_3O)_2Mg_6Si_8O_{22}(OH)_2$ or $(H_2O)_2Mg_6Si_8O_{20}(OH)_4$, depending how H_2O was assumed to be present. Whereas they favor the former on the basis of a unique but poorly resolved IR band, Miller *et al.* [11] noted that Bauer and Sclar also gave IR data that were unique for H_2O. TG and DTG show only a single

interlayer dehydration event [27, 29], suggesting that weight-loss involves only one H_2O species.

HP-DTA data

DTA curves for open-capsule runs (Fig. 14) show broad peaks, sharpening somewhat at higher pressures. Because the DTG evidence indicates predominately a single interlayer water species, these broad peaks suggest an increase in P_{H_2O} during dehydration, which causes dehydration to occur over a relatively large pressure range at lower pressures. Dehydration peaks in closed-capsule runs, at $P_{H_2O} = P_{total}$ are significantly sharper (Fig. 15). The run products are talc; therefore, the dehydration reaction is 10Å phase ↔ talc + V.

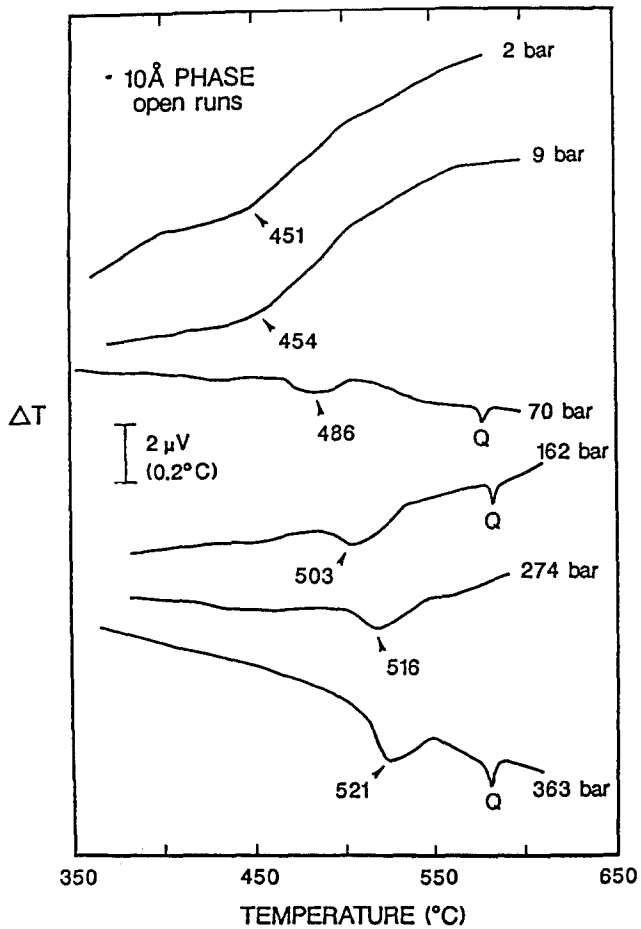

Fig. 14 HP-DTA patterns of the dehydration reaction of the 10Å phase, using open-capsule runs. The arrows indicate the peaks. *Q*, representing the low quartz-high quartz inversion, is used for calibration

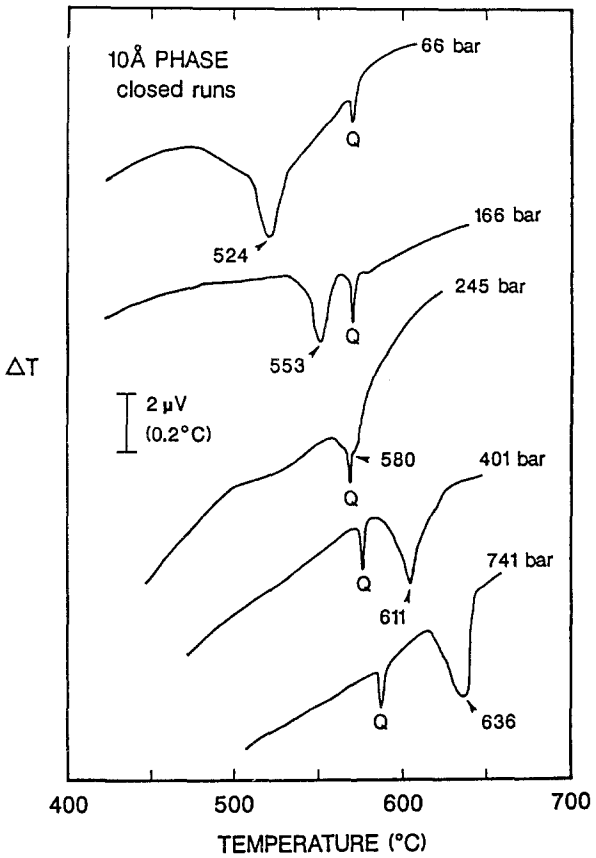

Fig. 15 HP-DTA patterns of the dehydration reaction of the 10Å phase, using closed-capsule runs. The arrows indicate the peaks. (*Q*, see Fig. 14)

Discussion

The *PT* relations of the dehydration reaction and $(L, V)_{H_2O}$ are shown in Fig. 16. Note that the dehydration reaction is observed well above the critical point of water. This suggests that the H_2O molecules are strongly bonded to the structure. This is consistent with the high temperatures needed for dehydration.

The van't Hoff equation can be applied to stable or metastable equilibria, but not to kinetically-controlled events. Because the 10Å phase is not stable at the pressures examined here, it is necessary to establish whether the dehydration represents a metastable reaction or an event that is kinetically controlled. Miller *et al.* [11] argued that the reaction is metastable on the basis that kinetically controlled reactions are (1) usually not pressure sensitive, and (2) are not affected greatly by differences in water vapor pressure. In addition, this reaction is similar

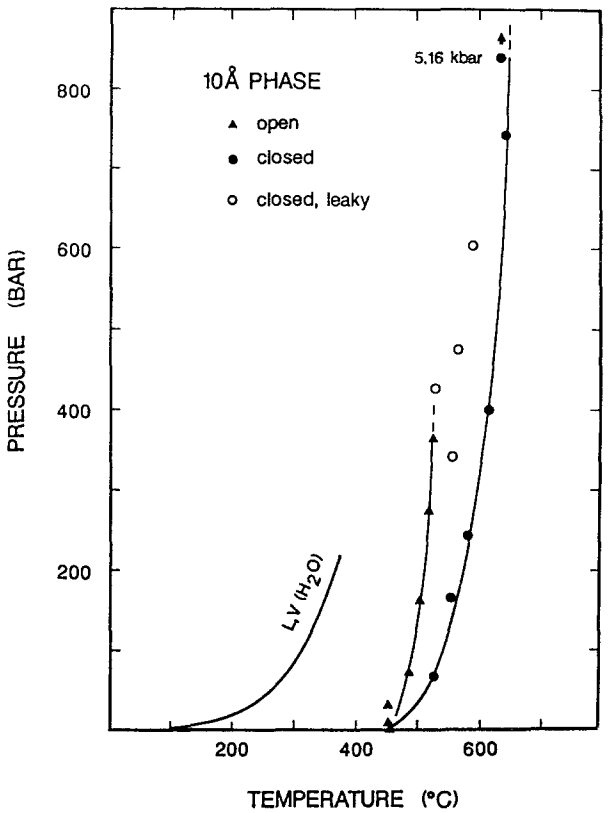

Fig. 16 *P–T* relations of the dehydration reaction of the 10Å phase. The boiling reaction of water $(L, V)_{H_2O}$ [14] is shown for comparison

to other stable and metastable phyllosilicate mineral reactions showing a strong and monotonic increase of dehydration with pressure, as is illustrated by the data in a $\ln P$–$1000/T$ space (Fig. 17).

A ΔH_{iw} value for this reaction of 200± 20 kJ/mole was obtained. This value is similar to those for the loss of a hydroxyl group (see below), rather than for interlayer water-loss. This suggests that H_2O in this structure does not reside in the interlayer as either H_2O or as the more unstable H_3O^+ molecule. Instead, considerable interaction between the oxygen and its neighbors is required to achieve the high bond energies indicated by the enthalpy of dehydration. Miller *et al.* [11] suggested that hydrogen resonance acts to bond strongly the oxygen to the interlayer, allowing the momentary formation of OH, H_2O, and H_3O^+ molecules as required by the infrared data [27]. The model is consistent also with the thermogravimetric data, which show essentially a single interlayer dehydration event.

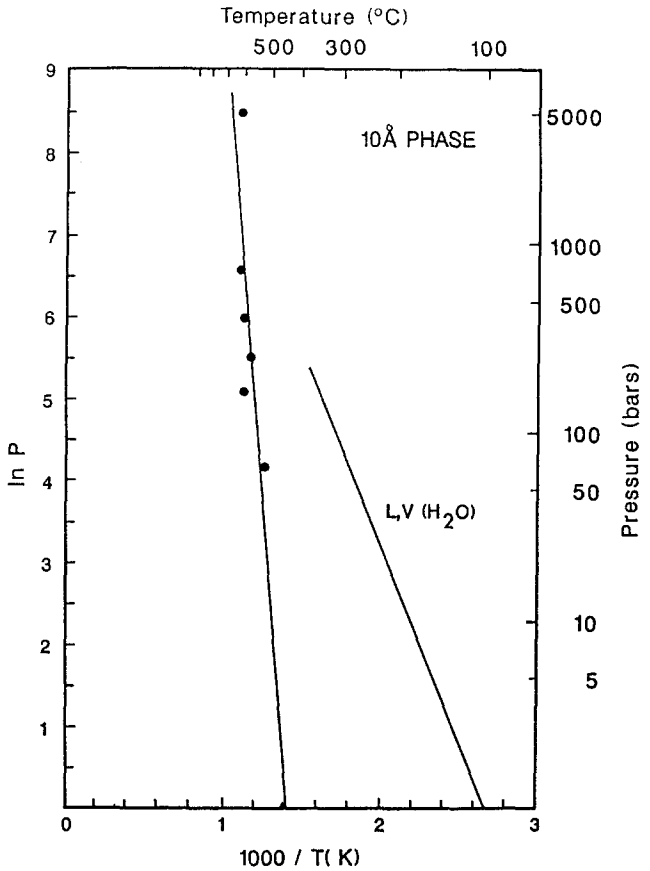

Fig. 17 A ln$P$–1000/T projection of the dehydration reaction of the 10Å phase. The boiling reaction of water $(L, V)_{H_2O}$ [14] is shown for comparison

Additional support for the assumption that the dehydration reaction is metastable is that in PT space it can be considered the metastable extention of the stable reaction: 10Å phase ↔ talc + V encountered at 600–700°C and 50–70 kbar [29]. It should be noted, however, that Bauer and Sclar [26, 27] found this reaction at a maximum temperature of 535°C.

Concluding comments to Part I

HP-DTA provides greater and more unique information than traditional DTA methods because of the ability to form a pressure-temperature grid. Further improvements involve the use of closed capsules, which allow experiments to be run

under fluid-saturated conditions. Although dehydration reactions in phyllosilicates may occur at relatively low temperatures that interfere with a peak for the boiling of water, it is still possible to extract information directly from the near superposed peaks. Part II will show, however, that it may be possible also to select different pressures to separate thermal events of two phases with coinciding or nearly coinciding peaks, providing that the phase relations are sufficiently different.

* * *

Support for this work was provided by the Petroleum Research Fund of the American Chemical Society under grants #21974-AC8-C and 20016-AC2, and the National Science Foundation under grants #EAR-9003688 and EAR-8816898.

References

1 W. W. Wendlandt, in 'Thermal Analysis' 3rd Edit. Wiley & Sons, N. Y. 1986.
2 A. F. Koster van Groos, Jour. Phys. Chem., 83 (1979) 2976.
3 S. Guggenheim and A. F. Koster van Groos, J. Thermal Anal., (in press) Part II of present paper.
4 A. F. Koster van Groos and S. Guggenheim, in 'Thermal Analysis in Clay Science' J. W. Stucki, D. Bish and F. A. Mumpton, eds., Clay Minerals Society, Boulder, 1990.
5 J. R. Holloway, in 'Research for High Pressure and Temperature' G. C. Ulmer, ed., Springer-Verlag, N. Y. 1971 p. 217.
6 H. S. Yoder Jr., Trans. Amer. Geophys. Union, 31 (1950) 827.
7 A. F. Koster van Groos and J. P. ter Heege, Jour. Geol., 81 (1973) 717.
8 H. van Olphen and J. J. Fripiat, Eds., Data Handbook for Clay Materials and other Non-metallic Minerals, Pergamon Press, Oxford 1979.
9 G. W. Brindley, D. L. Bish and H. Wan, Mineral. Mag., 41 (1977) 443.
10 C. B. Sclar, A. I. Benimoff and A. L. Begley, Eos, Trans. Amer. Geophys. Union, 68 (1987) 433.
11 A. K. Miller, S. Guggenheim and A. F. Koster van Groos, Amer. Mineral., 76 (1991) 106.
12 A. F. Koster van Groos and S. Guggenheim, Amer. Mineral., 69 (1984) 872.
13 L. Heller, V. C. Farmer, R. C. MacKenzie, B. D. Mitchell, and H. F. W. Taylor, Clay Minerals Bull., 5 (1962) 56.
14 J. H. Keenan, F. G. Keyes, P. G. Hill and J. G. Moore, Eds. Steam Tables: Thermodynamic Properties of Water Including Vapor, Liquid and Solid Phases, Wiley, N. Y. 1978.
15 A. F. Koster van Groos and S. Guggenheim, Clays Clay Minerals, 34 (1986) 281.
16 A. F. Koster van Groos and S. Guggenheim, Amer. Mineral., 72 (1987) 292.
17 R. E. Grim, Clay Mineralogy. McGraw-Hill, N. Y. 1968 p. 288.
18 V. C. Farmer, Soil Sci., 112 (1971) 62.
19 P. F. Low, Soil Sci. Soc. Amer. Jour., 43 (1979) 651.
20 B. G. Ellis and M. M. Mortland, Amer. Mineral., 47 (1962) 371.
21 G. M. Anderson, in 'Applications of thermodynamics to petrology and ore deposits', H. J. Greenwood, ed., Mineralogical Association of Canada, Toronto 1977 p. 17.
22 H. C. Helgeson and D. H. Kirkham, Amer. J. Sci., 274 (1974) 1089.
23 R. A. Robie, B. S. Hemingway and J. R. Fisher, U. S. Geol. Surv. Bull., 1452 (1978).
24 A. K. Miller, S. Guggenheim and A. F. Koster van Groos, Clays Clay Mineral., 39 (1991) 127.

25 C. B. Sclar, L. C. Carrison and C. M. Schwartz, Trans. Amer. Geophys. Union, 46 (1965) 184.
26 J. F. Bauer and C. B. Sclar, in 'High-Pressure Science and Technology' (proceedings Sixth AIRAPT Conference), K. D. Timmerhaus and M. S. Barber, eds. Plenum Press, N. Y. 1979 p. 144.
27 J. F. Bauer and C. B. Sclar, Amer. Mineral., 66 (1981) 576.
28 B. W. Evans and S. Guggenheim, in 'Hydrous phyllosilicates and other non-mica layer silicates' S. W. Bailey, ed., Mineralogical Society of America (1988) 225.
29 K. Yamamoto and S. Akimoto, Amer. Jour. Sci., 277 (1977) 288.
30 S. W. Bailey, in 'Crystal Structures of Clay Minerals and their X-ray Identification' G. W. Brindley and G. Brown, eds., Mineralogical Society of Great Britain, London 1984 p. 1.

Zusammenfassung Hochdruck-DTA Ergebnisse werden verwendet, um die Dehydratationsreaktionen für die tonartigen Materialien von Na-reichem Montmorillonit, von K-, Ca- und Mg-substituiertem Montmorillonit, Kerolit und einer durch Konfektionieren von Talkum/Glimmer mit überschüssigem Wasser entstandenen Hochdruckphase zu beschreiben. Da für Flüssigkeiten verschlossene Kapseln verwendet werden können, kann die Rolle von Wasser in diesen Reaktionen festgestellt werden. Ein anderer Beitrag (Teil II) beschreibt die Anwendung von HP-DTA bei der Untersuchung der Dehydroxylierungsreaktionen in diesen Materialien.